water

Article

Spatiotemporal Patterns of Hydrological Variables in Water-Resource Regions of China

Chao Zang [1], Huan Liu [2,*], Guotao Cui [3] and Jing Liu [4,5]

1 Graduate School of Life and Environmental Sciences, University of Tsukuba, Tsukuba 305-8571, Japan
2 The State Key Laboratory of Simulation and Regulation of Water Cycle in River Basin (SKL-WAC), China Institute of Water Resources and Hydropower Research (IWHR), Beijing 100038, China
3 School of Geography and Planning, Sun Yat-sen University, Guangzhou 510275, China
4 College of Water Resources, North China University of Water Resources and Electric Power, Zhengzhou 450001, China
5 School of Geography, Earth and Environmental Sciences, University of Birmingham, Birmingham B15 2TT, UK
* Correspondence: liuhuan@iwhr.com

Abstract: The spatiotemporal patterns of key hydrological variables across China were illustrated based on the developed Water and Energy Transfer Processes model in China (WEP-CN model). Time series of four key hydrological variables, namely, precipitation (*P*), runoff (*R*), infiltration (*Inf*), and actual evapotranspiration (ET_a), were obtained over 60 years. Then, the temporal trends and spatial differences of these variables were analyzed using the Mann-Kendall and linear methods on a national scale and on the water resource regional scale. Moreover, we explored the drivers and constraints for changes in *R*, *Inf*, and ET_a. The results showed: (1) Based on the coefficient of variations of *P* (5.24%), *R* (11.80%), *Inf* (2.57%), and ET_a (3.77%), *R* was more fluctuating than the other variables. (2) These variables followed a similar trend of gradually decreasing from the southeast coast to the northwest inland. (3) Changes in *R* and *Inf* were caused mainly by *P*, having correlation coefficients with precipitation of 0.74 and 0.73, respectively. The ET_a was constrained by a combination of *P* and energy. The results improved the refined and quantitative research on hydrological processes in China, identified the differences in hydrological variables between water-resource regions, and provided a useful supplement to the research of the large-scale hydrological process.

Keywords: hydrological variables; large-scale modeling; temporal trend; spatial patterns; WEP-CN model

Citation: Zang, C.; Liu, H.; Cui, G.; Liu, J. Spatiotemporal Patterns of Hydrological Variables in Water-Resource Regions of China. *Water* **2023**, *15*, 1643. https://doi.org/10.3390/w15091643

Academic Editors: Jianhua Xu and Zhongsheng Chen

Received: 3 March 2023
Revised: 8 April 2023
Accepted: 20 April 2023
Published: 23 April 2023

1. Introduction

Climate change is not only disrupting the production systems and ecosystem [1] but also causing changes in resource availability, such as natural hydrological resources [2–4]. Thus, it is necessary to explore large-scale hydrological variable patterns within the framework of long-term time series. The natural hydrological cycle controls the formation and evolution of renewable freshwater resources for human survival and development [5,6]. Obviously, the appropriate planning and management of water resources require a solid understanding of the hydrological process and its dynamics. Oki and Kanae [6] stated that "if the water cycle is managed wisely, renewable freshwater resources (RFWRs) can cover human demand far into the future". Consequently, numerous studies have attempted to quantify and predict the changing characteristics of key hydrological variables dominated by precipitation, evaporation, and runoff. Traditional hydrological research, however, often is focused on the catchment scale [7,8]. The hydrological model is valued as a tool. It was developed from the previous lumped models to the physically based distributed model, such as the TOPMODEL, MIKESHE, and soil and water assessment tool model [9]. In recent years, increasing pressure on water use at regional and national scales has forced people to advance their understanding of hydrological processes from a macroscopic view. Consequently, large-scale hydrological research with multiple catchments has become a popular research area. As pointed out by Kingston [10], "taking a large-scale perspective can bring significant benefits to our understanding of hydrological processes under change".

Two main approaches, the statistics-based and model-based methods, are widely used to understand the large-scale hydrological cycle and its variables. The statistics-based method generally uses satellite remote sensing data on precipitation, evaporation, and water resources at the continental and even global scale. For example, a large number of satellite/reanalysis-based precipitation products have been applied in global meteorological and hydrological analyses [11,12]. The reference evapotranspiration has been estimated from remote sensing–based surface temperature and local standard meteorological data [13]. An application of the Gravity Recovery and Climate Experiment (GRACE) satellites revealed regional depletion of groundwater resources [14,15]. Despite the advantages of these satellite products over gauge-based observations in terms of spatial coverage, they have large uncertainties and errors arising from sensor deficiencies, retrieval algorithms, and discordant data resolution [16,17]. The model-based methods rely mainly on large-scale hydrological modeling, which has made significant progress and has turned into an interesting field. Numerous large-scale land surface hydrological models also have emerged to investigate changes in hydrological characteristics, including the variable infiltration capacity (VIC) [18], WaterGAP [19], WASMODM [20], the mesoscale Hydrologic Model (mHM) [21], and E-HYPE [22]. Typically, a grid with a resolution of tens or even hundreds of kilometers has been used as the computation unit in these models, which has resulted in the distortion of the river network, flow path, and land cover. Consequently, we have failed to achieve a refined understanding of the spatiotemporal variation characteristics of hydrological variables in large-scale areas. Therefore, many researchers have attempted to improve computation units and parameters of the existing physically based hydrological models to extend their applications from small- and medium-scale regions to large-scale regions [23–25].

China covers a land area of about 9.6 million km^2, including many river basins and various geophysical and climatic zones. The hydrological variables in China, however, have not yet been comprehensively investigated because of the lack of a detailed national hydrological model and operating environment. Some studies have examined a single variable in China, such as estimating actual evapotranspiration [26,27], analyzing reference evapotranspiration [28], and discussing the spatial patterns of precipitation [29,30]. Feng et al. [31] and Bai et al. [32] used GRACE data to present the spatiotemporal patterns of groundwater storage in China. Analysis of runoff characteristics on a large scale with different spatiotemporal resolutions continues to be a popular research topic [33–35]. Using the VIC model, Miao and Wang [36] produced a flux database of the key hydrological variables in China from 1961 to 2017, including runoff, evapotranspiration, soil moisture, and water storage. This study calculated only the runoff flux of the nine largest rivers in China, and low-resolution data constrained the investigation of the spatial heterogeneity of runoff flux. Sun et al. [37] examined spatiotemporal shifts of evapotranspiration and runoff across 9 Class I Water Resource Regions of China, which is unsatisfactory in terms of spatial coverage and the number of hydrological variables.

To comprehensively describe and analyze the spatial heterogeneity of hydrological processes in China, we developed the Water and Energy Transfer Processes model in China (WEP-CN), a high-resolution, physically based hydrological model (see details in Section 2.3). The model better implements the simulation of the hydrological variables on a national scale. In this study, we applied this model and combined statistical methods to answer several questions: (1) what are the temporal trends in key hydrological variables of China in recent decades? (2) Where are the spatial differences in these variables among hundreds of water resource regions? (3) What are the drivers and constraints that affect the changes in these hydrological variables? We effectively realized the high-resolution display of key hydrological cycle variables, including precipitation (P), infiltration (Inf), evaporation

(*E*), and runoff depth (*R*), across the country. The results systematically analyzed the evolutionary characteristics of the water cycle at the national and different water-resource region scales and identified the variability among water-resource regions. The research results are a useful supplement to the research of the national-scale hydrological process and provide a new reference for the high-resolution analysis of national-scale hydrological variables through model-based methods.

2. Materials and Methodology

2.1. Study Area

China (N:3°52′–N:53°34′, E:73°40′–E:135°05′) is situated in the southeastern part of the Eurasian continent, with an area of 9.6 million km^2. The mean annual temperature varies from −5.4 °C to 27.8 °C, and the mean annual precipitation is 649.8 mm, with an extremely uneven distribution [38]. Based on the integrity of the river system and water management requirements, China can be classified according to 10 Class I Water Resource Regions (WWRs), 80 Class II WRRs, and 210 Class III WRRs [39–41]. The 10 Class I WRRs are shown in Figure 1 and include Songhua River Basin (SRB), Liao River Basin (LRB), Haihe River Basin (HRB), Yellow River Basin (YRB), Huai River Basin (HURB), Yangtze River Basin (YZRB), Pearl River Basin (PRB), Southeast River Basin (SERB), Southwest River Basin (SWRB), and Northwest River Basin (NWRB). Generally, the main rivers in China flow from west to east, determined by elevation differences, suggesting that most river basins have an upstream and downstream relationship. Six Class I WRRs (i.e., SRB, LRB, HRB, YRB, HURB, and SWRB) are located in the north of China, and the remaining four are located in the south. Figure 1 shows the distribution of China's WRRs.

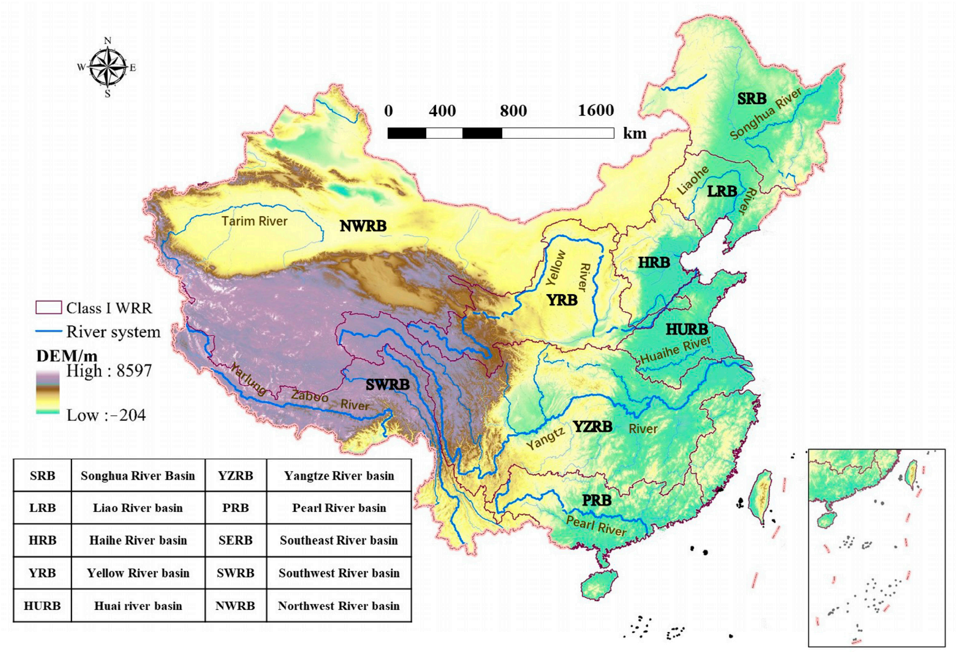

Figure 1. Distribution of main rivers and Class I WRRs of China.

2.2. Data Sources

Meteorological data were provided by the National Meteorological Information Center of China [42]. The data on river runoff, soil moisture content, and groundwater table were provided by the Annual Hydrological Report of China [43], the Second National Water Resources Survey, and the China Hydrological Yearbook, respectively. All data entered into the WEP-CN model have been processed into grids with a spatial resolution of 1 km × 1 km. For detailed data and model validation, refer to Liu et al. [44]. The model provided more than 20 hydrological variables. We selected the key variables (i.e., P, ET_a, R, Inf) to be aggregated and explored data on an annual scale from 1956 to 2017 over China.

2.3. Methodology

2.3.1. WEP-CN Model

Taking China as the study area, we succeeded in developing a high-resolution, physically based hydrological model running nationally. First, using the improved WEP-CN method of river system generation and sub-watershed division, we obtained a well-defined simulation area with 19,406 sub-watersheds and 86,406 contour belts [45]. Second, we adopted the three-dimensional interpolation method with consideration of elevation effects to interpolate precipitation and air temperature combined with the satellite products. Similarly, we obtained vegetation data for the different elevation zones using satellite remote sensing data. Third, we improved the numerical simulation of soil moisture movement in the vadose zone. We quantitatively analyzed the effects of karst development, soil swelling deformation, and soil freezing and thawing on soil moisture movement and modified the related parameters.

We calculated evapotranspiration according to the Penman-Monteith equation [46,47]. The water balance approach and a multilayered Green-Ampt model [48] can be used to simulate saturation-excess runoff and the infiltration excess runoff generation, respectively. We computed overland flow and river flow using a one-dimensional kinematic wave approach and simulated groundwater flow using the Boussinesq equations [24]. The main components of the WEP-CN model are shown in Figure 2. For model calibration and validation, we performed continuous simulations of 62 years (1956–2017) for various land cover conditions. By comparing simulated and statistical monthly streamflow at the 203 hydrological stations across the country, the results showed that the model had higher accuracy. Focusing on the validation period, the Nash-Sutcliff Efficiency (NSE) was larger than 0.7 at 80% of the stations, and the absolute value of relative error (RE) was less than 10% at 95% of the stations, as listed in Table 1. For more details about this model, refer to Liu et al. [44].

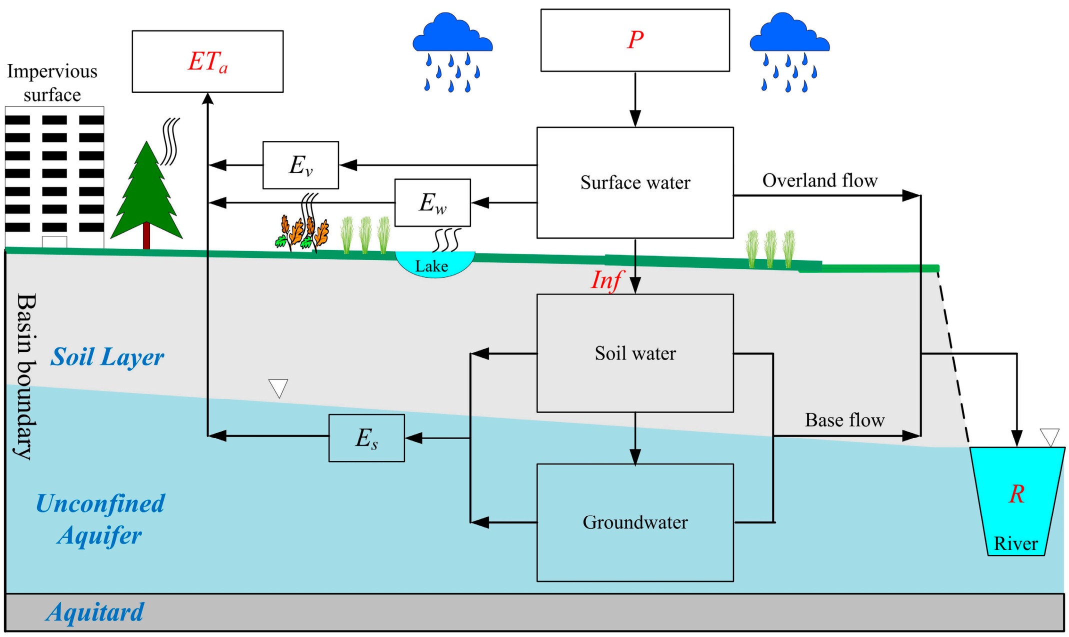

Figure 2. Schematic diagram of main components in the WEP-CN model. P is precipitation (mm), ET_a is actual evapotranspiration (mm), E_w is evaporation (mm) of surface interception and waterbody, E_v is vegetation transpiration (mm), E_s includes soil evaporation (mm) and phreatic evaporation (mm); R is runoff depth (mm), including overland flow and base flow; Inf (mm) is infiltration.

Table 1. Calibration and validation results of 203 hydrological stations in China.

WRRs	Total Number of Stations	Calibration Period (1956–1980)				Validation Period (1981–2000)			
		$NSE > 0.7$		$\lvert RE \rvert < 10\%$		$NSE > 0.7$		$\lvert RE \rvert < 10\%$	
		NUM	PCT	NUM	PCT	NUM	PCT	NUM	PCT
China	203	165	81%	184	91%	163	80%	193	95%
SRB	28	20	71%	26	94%	18	63%	26	94%
LRB	17	12	73%	17	100%	14	82%	17	100%
HRB	16	14	89%	12	78%	12	75%	14	89%
YRB	31	22	71%	29	93%	22	71%	29	93%
HURB	12	11	90%	10	80%	8	70%	12	100%
YZRB	47	45	96%	41	88%	47	100%	43	92%
SERB	12	12	100%	12	100%	12	100%	12	100%
PRB	25	25	100%	20	80%	23	90%	20	80%
SWRB	10	6	64%	8	82%	7	73%	10	100%
NWRB	5	3	67%	3	67%	3	67%	3	67%

Note: NUM and PCT represent the number of qualified stations and their proportion in the total number.

2.3.2. Trend Analysis

We used the Mann-Kendall (M-K) trend test [49] to quantify the significance of temporal trends for hydrological variables, which can be intuitively expressed by a statistical value. The M-K trend test is not affected by the actual distribution of the data, is not affected by missing data or by the irregular spacing of the time points of measurement and is less sensitive to outliers. This method has been used widely to evaluate the significance of trends in hydrometeorological time series [50,51]. The calculation process is as follows:

$$S = \sum_{a=1}^{n-1} \sum_{b=a+1}^{n} \text{sgn}(x_b - x_a); \quad \text{sgn}(x_b - x_a) = \begin{cases} -1, & \text{if } x_b - x_a < 0 \\ 0, & \text{if } x_b - x_a = 0 \\ +1, & \text{if } x_b - x_a > 0 \end{cases} \tag{1}$$

where S denotes the statistic variables of the M-K trend test, n is the number of detected data series, and x_a and x_b are the data values in time series a and b ($b > a$), respectively.

$$Z = \begin{cases} \frac{S+1}{\sqrt{Var(S)}}, & \text{if } S < 0 \\ 0, & \text{if } S < 0 \\ \frac{S-1}{\sqrt{Var(S)}}, & \text{if } S > 0 \end{cases}; \quad Var(S) = \frac{n(n-1)(2n+5) - \sum_{p=1}^{q} t_p(t_p - 1)(2t_p + 5)}{18} \tag{2}$$

where Z is the standard normal test statistics. Positive values of Z_S show increasing trends, whereas negative Z values indicate decreasing trends; t_p denotes the number of ties up to sample p; and q is the number of tied groups. If $\lvert Z \rvert > Z_{1-\alpha/2}$, the null hypothesis is rejected, and the variable exhibits a significant trend at the α level. In this study, Z values of precipitation, temperature, runoff depth, infiltration, actual evapotranspiration, and internal renewable water resources (*IRWRs*) were denoted as Z_p, Z_t, Z_r, Z_{inf}, Zet_a, and Z_{irwr}, respectively. Because we used a two-sided test, the threshold for the significance test at the 0.05 level was 1.96. In addition, we also used linear trend analysis in this study to compare and contrast the M-K trend analysis.

3. Results

3.1. Mean Spatial Pattern of Key Hydrological Variables

Figure 3 shows the spatial distribution of the long-term means (1956–2017) of the key hydrological variables (i.e., precipitation, runoff, infiltration, and actual evapotranspiration) in China. All variables decreased from the southeast coast to the northwest inland, showing regional differences. Because the southeast areas are situated closer to the coast, compared with the northwest inland, the hydrological variables are more likely to be affected by the East Asian monsoon. As shown in Figure 3a, the maximum value area of P was distributed in the southwest regions (SWRB), which was caused by the prevailing Indian monsoon. Compared with the other three variables, Figure 3b shows that the area with a small R (<100 mm) in northern China was extremely large, which can be explained by the following: (1) the regions with R less than 100 mm overlapped with the regions with P less than 800 mm, as P is the major factor restricting R; and (2) most of the P infiltrated and evaporated because of low soil moisture, small air humidity, and mechanism of the runoff yield, which was dominated by excess infiltration in the north [52].

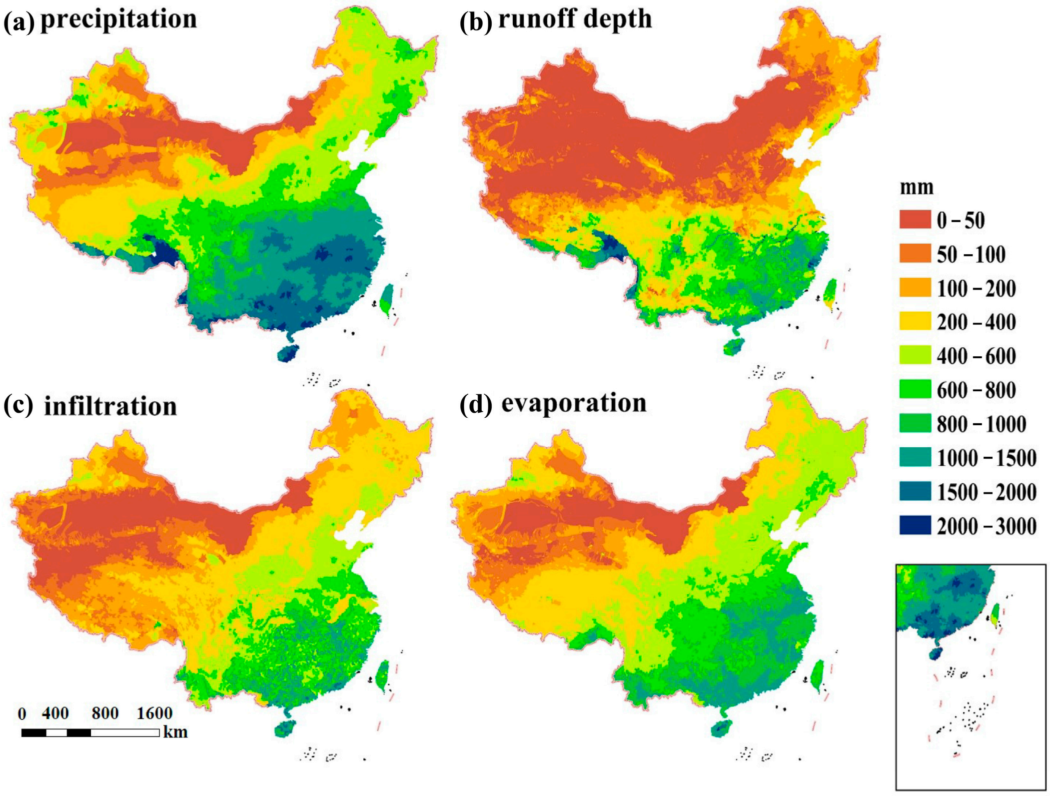

Figure 3. Mean spatial pattern of hydrological variables in China (1956~2017). (**a**) P; (**b**) R; (**c**) *Inf*, (**d**) ET_a.

Comparing Figure 3c with Figure 3d, in the area in northwest China, *Inf* and ET_a showed similarities in terms of magnitude and spatial pattern. We inferred that in northwest China (NWRB), most of the water that infiltrated into the soil was evaporated back into the atmosphere. However, in southeast China, which is covered by lush vegetation, ET_a was larger than Inf. It is likely that ET_a in southeast China is contributed by a combination of water in the soil layer and intercept water amounts by vegetation.

3.2. Temporal Changes of Key Hydrological Variables in China and Its WRRs

3.2.1. Temporal Trends of Hydrological Variables on National Scale

Figure 4 and Table 2 show the 62-year temporal trend of the key hydrological variables, averaged for the entire country. We analyzed the temporal trends with the linear regression and M-K trend test method. The 62-year average values of P, R, *Inf*, and ET_a over the country were 678.1 mm, 275.5 mm, 322.6 mm, and 431.6 mm, respectively. It should be emphasized that on a multi-year average national scale, P, R, and ET_a are not closed. This can be explained from two perspectives: (1) the water budget at the continental scale is not completely closed [53]; (2) Because the water equivalent of thaw and snowmelt are contributed to R and ET_a, their sum is larger than the P term. Variables P and R followed decreasing trends over 62 years, whereas the *Inf* and ET_a followed weak increasing trends.

The M-K test indicated that the trends of the four hydrological variables were not significant. Meanwhile, the four linear regression coefficients were not significantly different from the value 0 at the 0.05 level, according to the results of the t-test, which indicated that no significant trend existed in the time series of the four variables. The coefficient of variation (*CV*) of *P*, *R*, *Inf*, and ET_a was 5.24%, 11.80%, 2.57%, and 3.77%, respectively, which showed that *R* highly fluctuated, whereas *Inf* and ET_a were relatively stable. Additionally, *R* had a significant correlation with *P* in the time series, which passed the significance test at the 0.01 confidence level. Annual precipitation decreased at a rate of −0.35 mm/year (linear trend), suggesting a potentially higher frequency of drought. For example, an extreme drought event in Southwest China that occurred in 2009–2010 (the years with the lowest precipitation in Figure 4 was a "once-in-a-century drought" [54].

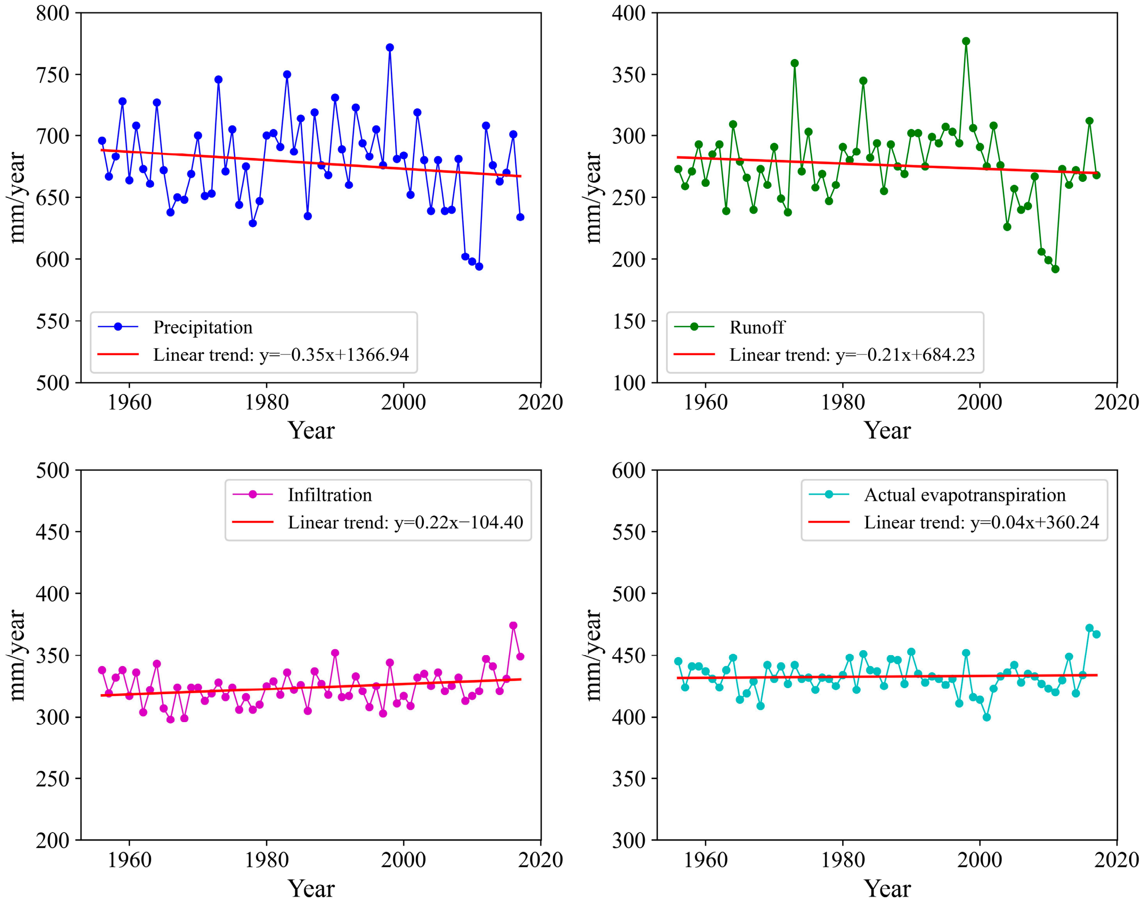

Figure 4. The linear trend of hydrological variables over China from 1956 to 2017.

Table 2. Statistics of key hydrological variables over time at national scales.

Variables	Mean (mm)	Z Values	*CV* (%)
P	678.1	−1.04	5.24
R	275.5	−0.44	11.80
Inf	322.6	−1.04	2.57
ET_a	431.6	1.03	3.77

3.2.2. Hydrological Variation and Its Differences among WRRs

We calculated trend changes on the scale of the Class III WRRs, as shown in Figure 5. We also presented the results on the scale of Class I WRRs. The changes in *P* across the country were spatially different. The *P* at most meteorological observation stations in the NWRB followed a significantly increasing trend ($Z_p > 1.96$). The increase in *P* effectively contributed to the abundance of water resources in NWRB. In addition, regions with increased P also included part of SWRB, downstream of YZRB, some areas in SERB, and PRB, but the results were not significant at the 0.05 confidence level. The regions that followed a decreasing trend of P ($Z_p < 0$) extended from the northeast to the southwest. These regions specifically included SRB, LRB, HRB, most of YRB, HURB, YZRB midstream, SWRB downstream, and part of PRB. Regions that showed a significant decline ($Z_p \leq 1.96$) were concentrated in the middle YZRB and scattered in other areas.

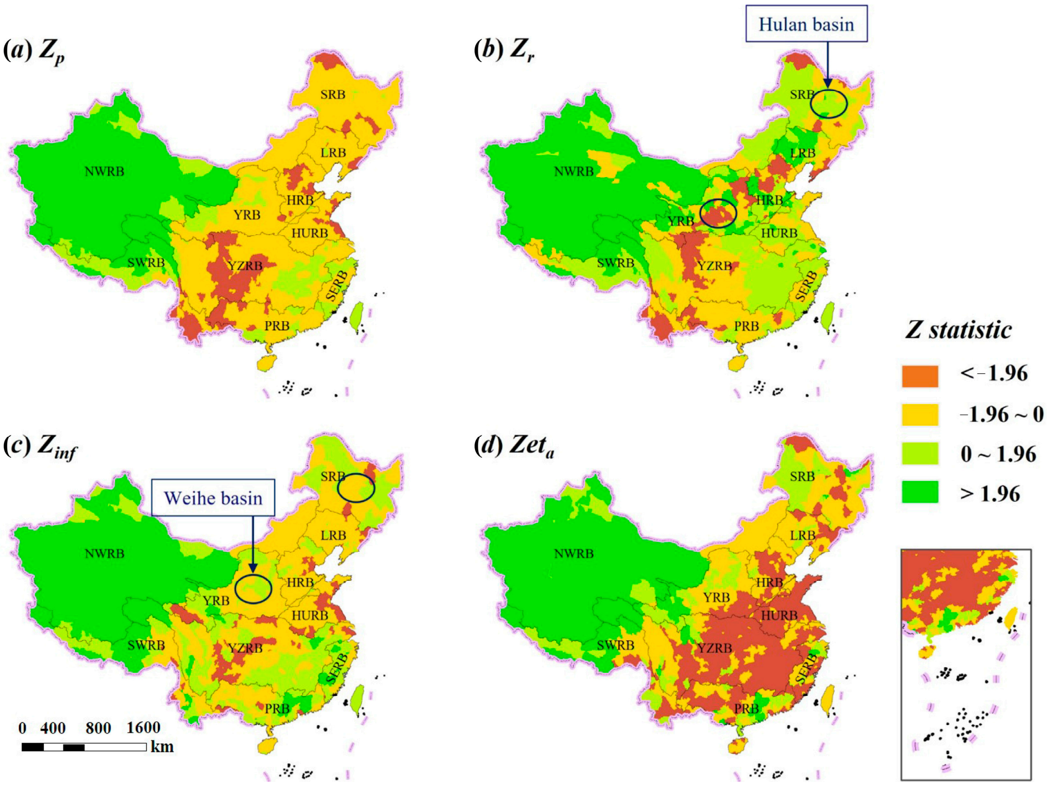

Figure 5. Spatial pattern of results for M-K trend test. (**a**) Z_p, (**b**) Z_r, (**c**) Z_{inf}, (**d**) Zet_a.

From the perspective of changes over the years, we identified differences in R for various regions, which can be roughly categorized into five areas. (1) Most areas of NWRB followed a significant increasing trend ($Z_r > 1.96$). (2) In the north-central area (parts of YRB and HRB), the changing trend of R show discretized spatial distribution, which irregularly switched between increasing and decreasing trends. (3) In the northeast area (SRB and LRB), increasing trends and decreasing trends presented clustered distributions, and the general pattern increased in the west and decreased in the east. (4) The southeastern area (downstream of YZRB, parts of HURB and SERB) showed an increasing tendency ($0 < Z_r < 1.96$). Conversely, (5) the southwestern areas (up and middle stream of YZRB and PRB; part of SWRB) showed a clustered decreasing tendency ($Z_r < 0$).

Analyzing these changes in infiltration volume from the interannual change trend, the results showed that its tendency to change (Figure 5c) overlapped well with the spatial distribution of Z_p (Figure 5a). Most of the Z_{inf} in NWRB showed a significant and concentrated increase, whereas this increase and decrease coexisted in other regions of China, which followed insignificant trends. Some scattered basins in southwestern and eastern regions showed significantly decreasing trends. The physical process of Z_{inf} change should be influenced by changes in precipitation and underlying surface (see Section 3.3.1)

According to the results of the M-K trend test, the ET_a in China has changed dramatically. These changes are concentrated and appear in large-scale areas with reduced ET_a that is significant ($Zet_a \leq 1.96$) from the central to the southeast (i.e., middle of HRB, middle and downstream of YZRB, HURB, and upstream of PRB). Most of the northwest

(NWRB) followed a significant trend of change that was diametrically opposed to that of the central and southeast regions. Other regions followed discretely increasing or decreasing trends, but clearly, more areas followed decreasing trends than increasing trends within an insignificant range.

Furthermore, we calculated the *CV* values of four key hydrological variables on Class III WRRs and summarized the variables in Class I WRRs, as listed in Table 3. Overall, the *CV* values for four variables in the Class I WRRs showed variability between north and south. Compared with the south, the *CV* values for *P* and ET_a were slightly greater in the north, whereas the *R* values were significantly greater. Conversely, the *CV* values for Inf were greater in the south.

Table 3. Coefficient of variations (*CV*) values of four key hydrological variables on Class III WRRs.

Class I WRRs	Location	Number of Class III WRRs	*CV* of *P*		*CV* of *R*		*CV* of *ET*		*CV* of *Inf*	
			Mean	Median	Mean	Median	Mean	Median	Mean	Median
SRB	North	18	5%	5%	6%	5%	3%	3%	6%	6%
LRB		12	4%	4%	7%	3%	2%	2%	4%	2%
HRB		15	8%	7%	16%	14%	6%	5%	3%	2%
YRB		29	5%	4%	16%	14%	4%	3%	3%	2%
HURB		14	6%	6%	10%	9%	3%	4%	6%	6%
NWRB		33	11%	11%	17%	18%	7%	8%	4%	3%
YZRB	South	45	3%	3%	4%	3%	2%	1%	8%	6%
PRB		10	3%	2%	2%	2%	1%	1%	8%	6%
SERB		20	3%	3%	2%	3%	2%	2%	8%	7%
SWRB		14	6%	4%	5%	2%	2%	2%	14%	10%

3.3. Drivers and Constraints for Changes in Key Hydrological Variables

3.3.1. Driving Forces for Changes in *R* and *Inf*

Changes in the climate and underlying surface were the main driving forces for variations in runoff and infiltration. The northwestern region presented a spatially continuous and large-scale trend in which both runoff and infiltration increased significantly. This likely was caused by increased *P* and thawing with warmer temperatures (*T*).

The size of *Z* values can reflect the significant degree of change in the variables over time. Therefore, we used the correlation analysis of the statistics (*Z* values) among different variables to determine whether a correlation existed between the intensity of change of the two variables. The meteorological data and hydrological data in 210 Class III WRRs were used, which were obtained from the data statistics of 19,406 sub-basins through model reanalysis. By analyzing the correlation between Z_p and Z_r, we found that they were significantly correlated at the 0.01 level with a linear correlation coefficient of 0.74; that is, a strong positive correlation existed in the intensity of change between *R* and *P* (see Figure 6a). We performed a similar correlation analysis between Z_p and Z_{rinf}. The result showed that they were significantly correlated at the 0.01 confidence level with a linear correlation coefficient of 0.73; that is, a strong positive correlation existed in the intensity of change between *Inf* and *P* (see Figure 6b).

We speculate that climate warming has caused the melting of glaciers and the thawing of frozen soils, which has increased water production in the regions. Although we confirmed a weak negative correlation between Z_t and Z_r when performing spatial correlation analysis in 210 Class III WRRs, which means we did not find direct evidence that warming was causing an increase in water production. A positive effect of temperature on *R* and *Inf*, however, could not be ruled out. Many studies [55–57] have reported that water production in this region has increased significantly with the melting of glacier snow in recent years. Conversely, it is unlikely that this change was caused by human activities because the vegetation coverage and population density are much lower in northwestern China than in other regions [58,59]. Southeast coastal areas (downstream of YZRB, parts of PRB, and

SERB) also have been affected by the P change ($0 < Z_p$), where both runoff and infiltration have shown an increasing tendency ($0 < Z_r$, Z_{inf}).

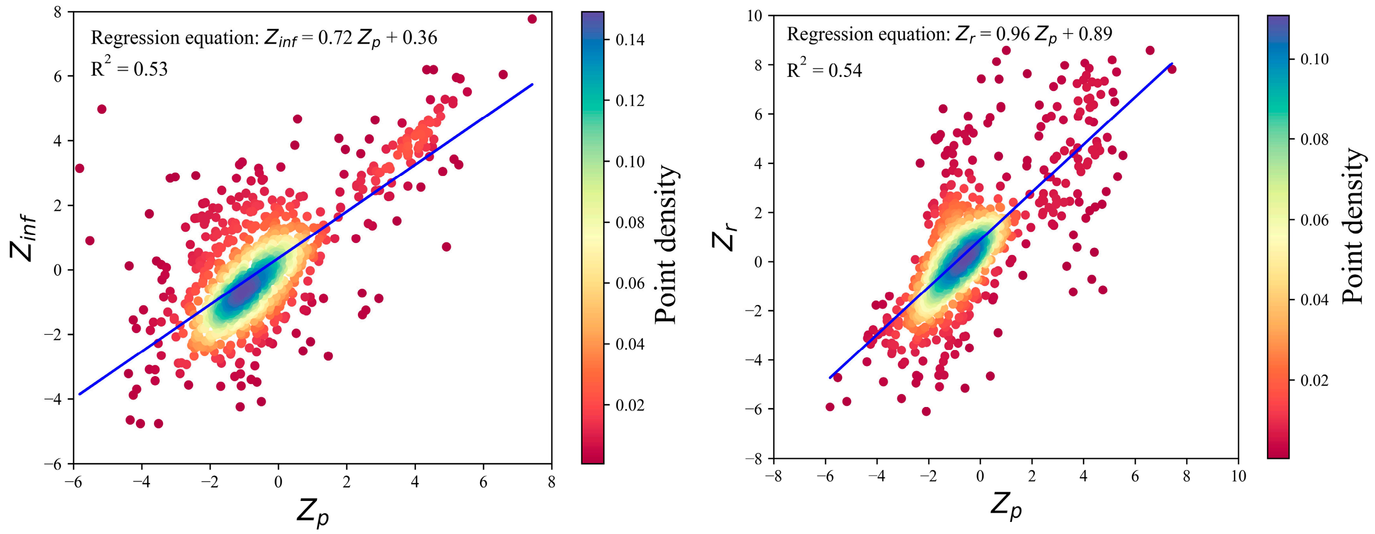

(**a**) (**b**)

Figure 6. Linear regression relationship and point density distribution map. (**a**): Linear regression relationship between Z_{inf} and Z_p; (**b**): Linear regression relationship between Z_r and Z_p.

Another phenomenon is that the driving force of underlying surface change was greater than that of the *P* variable. In those regions, runoff and infiltration roughly followed a reverse trend. This change in the underlying surface was reflected in forest areas, farming areas, and urbanization. A representative basin is the Hulan Basin (shown in Figure 5) in northeast China. With the recent implementation of a strategy to have a "large granary in the Northeast" [60], the agricultural area in the Hulan Basin has expanded rapidly. In 2015, the area of arable land increased by 56.58% compared with 1980. The proportion of forests decreased from 31.89% in 1980 to 28.34% in 2015, which directly increased the runoff and reduced the infiltration capacity [52]. In the Weihe Basin (shown in Figure 5), which is located in the middle of the YRB, soil and water conservation have been implemented for many years. The area of vegetation, such as forests and grasslands, has increased and has been accompanied by a decrease in bare land. This vegetation has increased the water conservation capacity of the basin, resulting in a decrease in runoff and an increase in infiltration [61,62].

We determined that the effects of climate change and underlying surface changes on runoff and infiltration are different in both spatial scales and intensity. On the national scale, the changes in runoff and infiltration driven by climate change (including precipitation and air temperature) were clearly more noticeable, as evidenced by the significant changes in the northwestern region. In contrast, the underlying surface changes due to human activities have been limited, and we identified only the impact of forest planting (Weihe Basin) and agricultural planting (Hulan Basin) in a scaled area. This result was consistent with the findings of an earlier investigation in 21 typical basins [52].

3.3.2. Constraints on Actual *ET*

Figure 7 shows the spatial pattern of the long-term mean of potential evapotranspiration (*PET*), which is the potential rate when sufficient water is available [63]. The spatial pattern of *PET* in China (Figure 7) followed the opposite spatial pattern of ET_a (Figure 3d), which indicated that water availability had played a critical role in constraining ET_a. This constraint, however, differed in the southern and northern regions. The results of the *t*-test for the correlation between ET_a and *P* showed that both variables had a significant correlation at the 0.01 confidence level in northern China (SRB, LRB, HRB, HURB, YRB, and NWRB) and southern China (SWRB, YZRB, SERB, and PRB). The regression coefficient (Figure 8), however, was greater in the north (0.78) than in the south (0.57). This means that P in the north placed a greater constraint on ET_a than it did in the south. This finding was consistent with the perspective [64] that the north has water-limited ET_a and the south has energy-limited ET_a based on the concept of the Budyko framework [65].

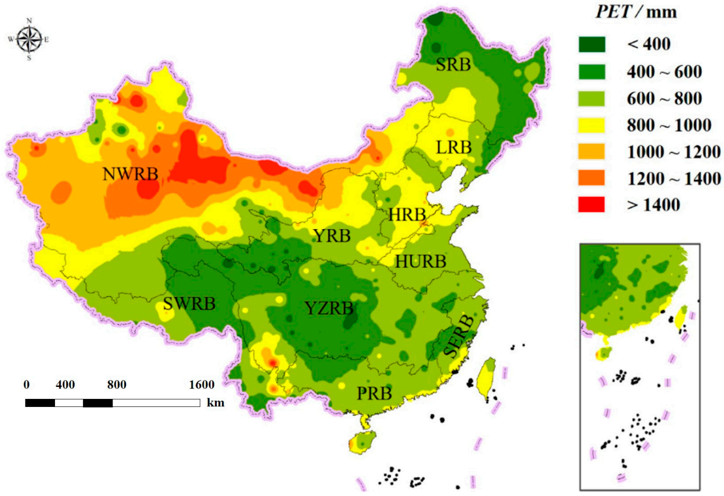

Figure 7. Spatial distribution of the mean *PET*.

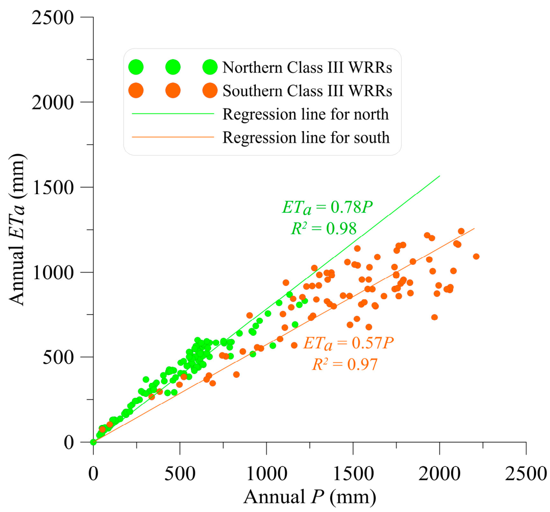

Figure 8. Linear regression relationship between ET_a and P in north and in south Class III WRRs. R^2 is the goodness of fit.

Figure 5d showed a significant reduction in large areas of the central region extending to southeastern regions, which was presumed to be related to a decrease in vegetation cover. Regarding forest evapotranspiration (Figure 9a), grassland evapotranspiration (Figure 9b), and surface interception and waterbody evaporation (Figure 9c), in the ET_a decreasing region, both ET_g and E_w followed a significant decreasing trend ($Z \leq 1.96$), and the range of declines in ET_f also was large. These results suggested the possibility that the vegetation cover of the region, particularly the area covered by grassland, declined significantly over the past few decades. The reduction in E_w (Figure 9c) may have been caused by the reduction in surface retention capacity because of changes in vegetation cover. This result was consistent with the finding that the vegetation coverage area, especially the grassland area in southeastern China, decreased significantly from 1980 to 2017 [66].

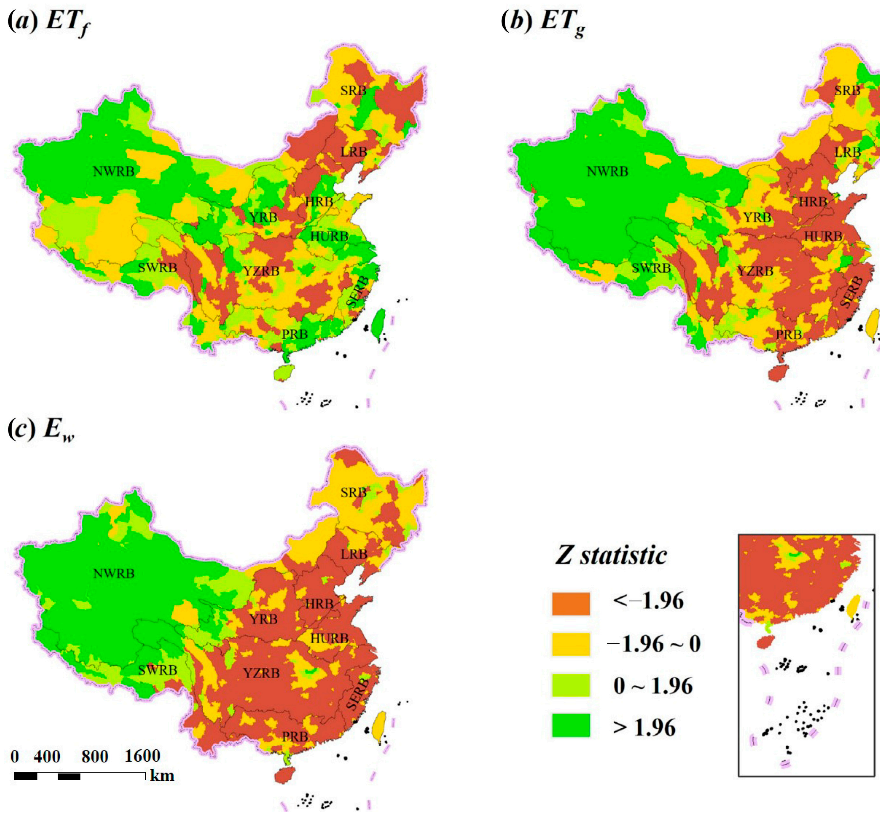

Figure 9. Spatial distribution of M-K trend test for (**a**) ET_f, (**b**) ET_g, and (**c**) E_w; ET is evapotranspiration and E is the evaporation; Subscript f, g, w means forest, grassland, and surface waterbody respectively.

The northwest region (NWRB) has the largest potential evapotranspiration in China. When the waterbody surface evaporation and interception evaporation (Figure 9c) in this area increase significantly, the forest transpiration also increases to a certain extent. Then, the ET_a of NWRB inevitably would follow a significant increasing trend (Figure 5d). The trend of precipitation has increased the amount of water available in NWRB. The melting of many glaciers and snow in the region, however, is another important factor that has been affecting water availability [67,68].

3.4. Assessment of Internal Renewable Water Resources

We evaluated the *IRWRs* of China based on the output variables of the WEP-CN model. The *IRWR* is defined as the average annual flow of rivers and recharge of aquifers generated from endogenous precipitation [69]. Here, $IRWR_a$ (m^3) and $IRWR_d$ (mm) were used, respectively. The results showed that the long-term mean value (1956–2017) of $IRWR_a$ in China was 2.81×10^{11} m^3/year, of which surface $IRWR_a$ was 2.71×10^{11} m^3/year and underground $IRWR_a$ was 0.82×10^{11} m^3/year. Note that the average overlap water between surface $IRWR_a$ and underground $IRWR_a$ was 0.72×10^{11} m^3/year.

In the spatial distribution of the Class III WRR scale, *IRWRs* gradually increased from northwest to southeast (Figure 10). The $IRWR_d$ of the northwestern region and the northern region adjacent to Mongolia was below 100 mm. The $IRWR_d$ of the northeast region was between 100 mm and 250 mm, but the $IRWR_d$ of the coastal areas was significantly higher than that of other areas, up to 700 mm. The southeast region had the most abundant $IRWR_d$, with an average annual value of about 1000 mm. In terms of time evolution, the $IRWR_d$ of HRB, SWRB, upper-middle stream of YZRB, and SRB decreased significantly ($Z_{irwr} \leq 1.96$), which likely was caused by the combined effects of climate factor and underlying surface change. The $IRWR_d$ of NWRB showed a significant increasing trend ($Z_{irwr} > 1.96$), possibly because of the melting of glaciers and the thawing of frozen soil.

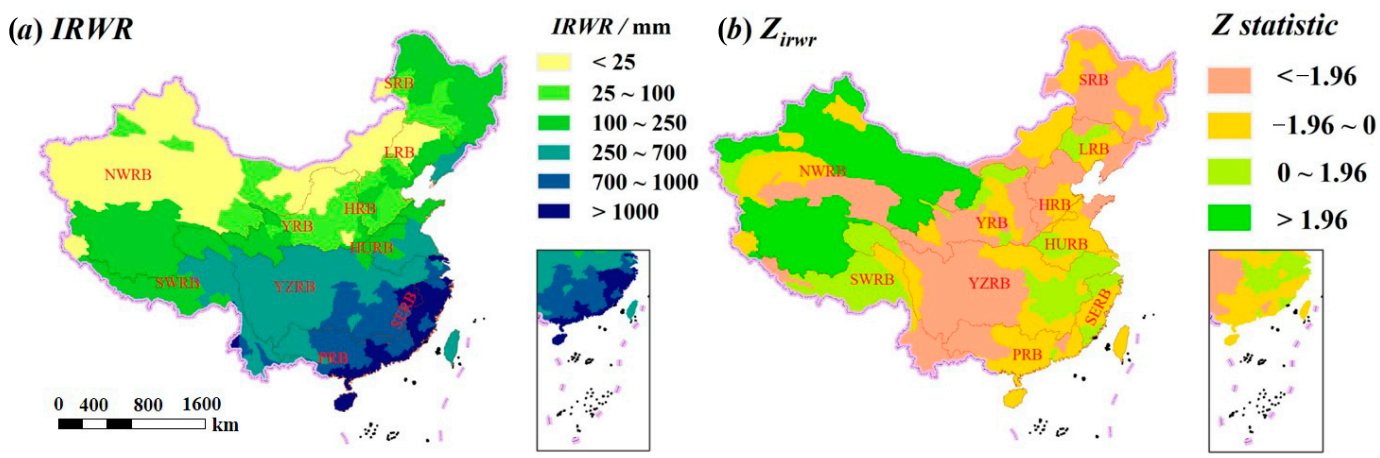

Figure 10. Spatial distribution of (**a**) $IRWR_d$ and (**b**) Z_{irwr}.

4. Discussion

The results of the study showed increased stress on water resources in the north. We obtained annual averages of $IRWR_d$ from the WEP-CN model. Because of the limitation of available data, the current water demand by Class I WRRs was represented by water consumption in 2019 [70]. Despite variances in the development and water use efficiency across WRRs, the data demonstrated the mismatches between water resources and population distribution in China. Figure A1 shows the 1956–2017 averages of $IRWR_d$ (mm) and 2019 water consumption (mm) on the national scale and the Class I WRR scale.

The results of the $IRWR_d$ ranking showed that water resources were far more abundant in the south than in the north because of the distribution characteristics of the hydrological variables, as has been widely reported [71,72]. In the north, the prospects for water surpluses to assist sustainable development were severe. The HURB has the highest water consumption, the HRB has the largest water deficit, and the YRB has been under a lot of water stress. Thus, the Chinese government has made a series of efforts in recent years to diminish this mismatch through water transfer projects [73] and water conservation policies [74].

Table A1 shows the interdecadal variation of *IRWRs* from 1956 to 2017. The interdecadal variability in the 1980–2000 period relative to the 1956–1979 period was represented as Case (1), and the interdecadal variability in the 2001–2017 period relative to the 1980–2000 period was represented as Case (2). In Case (1), the results showed a slight increase in the national average of *IRWRs*, with an increase of about 2%. The value with the largest increase (15%) was in the SRB, and the most significant decrease (40%) was in the HRB. In Case (2), the national average of *IRWRs* decreased by 5.2%. Except for the LRB, HURB, and NWRB, the rest of the Class I WRRs have decreased to varying degrees, ranging from 2.7% to 19.5%. The surface *IRWRs* on a national scale showed a 1.6% increase in Case (1) and a 4.1% decrease in Case (2). Correspondingly, the two values for the ground *IRWRs* were positive 3.3% and negative 8.3%. In summary, the two variabilities in surface *IRWRs* and subsurface *IRWRs* were relatively low at the national scale but showed considerable variability at the WRR scale, especially in the HRB.

Specifically, in the north, the IRWRs of the six Class I WRRs showed different water stress profiles. The most notable feature was a dramatic fall of *IRWRs* over more than half a century in the HRB, which was driven by a decrease in precipitation (see Figure 5a). The rate of decline of the *IRWRs* in the YRB has slowed down; however, when combined with the water consumption results shown in Table A1, it is apparent that the region is still facing greater water stress compared to the southern region. Hopefully, the execution of the "High-Quality Development of the Yellow River Basin" will break this cycle [75,76]. The *IRWRs* of the HURB followed a pattern of decreasing and then increasing. This unstable pattern of change has been highly detrimental to the sustainable utilization of the *IRWRs*, and the region was prone to the alternate occurrence of extreme drought and extreme flooding events [77]. Although NWRB showed an increase in *IRWRs*, to which the thawing processes made a non-negligible contribution, NWRB may continue to encounter water shortages as future thawing water decreases. Residents in the NWRB should be cautious when engaging in production activities. The reduction of runoff in recent years has contributed significantly to the severe reduction of the wetland area in SRB, and the shrinkage of the wetland has fed back into the reduced capacity to store runoff [78,79], which may result in potential disasters, such as flooding. Thus, the runoff storage capacity in SRB requires further attention.

In addition, it was found that the main results of this study were in good agreement with the published academic results [33,36,37,80,81] in terms of spatial distribution patterns and performed more superior in terms of spatial resolution. The main findings of this study are valid and credible and provide a useful supplement to the research of the large-scale hydrological process.

5. Conclusions

This study comprehensively presented the trends and spatial patterns of key hydrological variables in China over more than half a century. We have demonstrated that the four key hydrological variables (P, R, Inf, and ET_a) have followed spatial patterns of gradually increasing from the northwest to the southeast. Over 62 years, the key hydrological variables in different regions have revealed complex tendencies. The hydrological variables in the northwestern region have shown a concentrated and large-scale increasing trend, which we attributed to an increase in water availability caused by climate change. In the southeast coastal area, the increase in P contributed to the increase in the R and Inf, whereas ET_a has dropped unexpectedly as a result of the reduction of vegetation area.

Human activities have a significant effect on the key hydrological variables in local regions, but they are weaker in scope and intensity than climate change. Only if human activities (e.g., afforestation, expanding farmland) are implemented at a large scale will the hydrological variables be able to sufficiently respond to these driving forces on a relatively large basin scale.

Interdecadal variabilities of *IRWRs* in Class I WRRs suggested that the northern regions tend to face high water stress. In particular, the HRB and YRB, with high population density and active economic activity, have shown a sustained decline in *IRWRs*. The recent increase in *IRWRs* in the NWRB is potentially unsustainable. Reduced *IRWRs* in the SRB threatens local ecology and food security. In the future, several engineering and policy measures should be taken to optimize trade-offs and synergies between socioeconomic development and water resources and to explore pathways to sustainable development.

Author Contributions: C.Z.: Formal analysis, Writing—original draft and edit figures. H.L.: Methodology, Modeling, Writing—edit figures and tables, Resources, Validation, Supervision, Project administration. G.C.: Writing—review and editing. J.L.: Writing—review and editing. All authors have read and agreed to the published version of the manuscript.

Funding: This research was funded by the National Key Research and Development Program of China, grant number 2021YFC3200203; the National Natural Science Foundation of China (42001040); the National Natural Science Foundation of China (51909091); the China Scholarship Council (No. 202108410234); and the Basic Scientific Research Expense Project of IWHR (WR0145B072021, WR0145B022021).

Data Availability Statement: The data supporting the findings of this study are available from the corresponding author upon reasonable request.

Acknowledgments: The authors are grateful to the editors and anonymous reviewers for their insightful comments and helpful suggestions.

Conflicts of Interest: The authors declare that they have no known competing financial interests or personal relationships that could have appeared to influence the work reported in this paper.

Appendix A

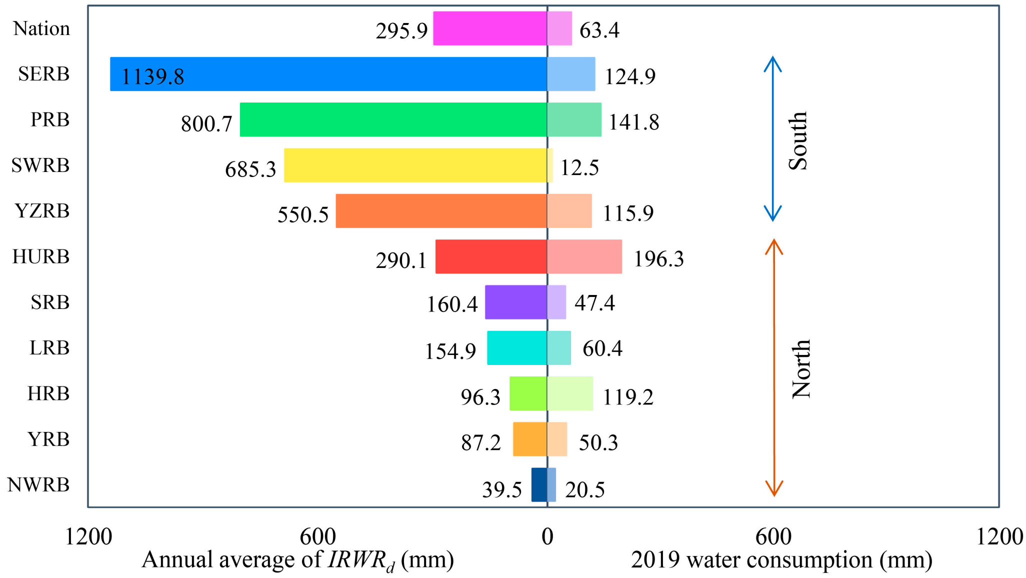

Figure A1. Annual averages (1956–2017) of $IRWR_d$ and 2019 water consumption.

Table A1. Interdecadal variabilities of *IRWRs* at the Class I WRR scale and national scale.

Class I WRRs/Nation	Variability of *IRWR*		Variability of Surface *IRWR*		Variability of Ground *IRWR*	
	Case (1)	Case (2)	Case (1)	Case (2)	Case (1)	Case (2)
SRB	14.51%	−11.19%	12.37%	−9.34%	14.49%	−12.49%
LRB	−10.96%	7.26%	−10.22%	7.61%	−4.31%	−1.71%
HRB	−37.4%	−19.48%	−38.07%	−6.41%	−31.55%	−29.43%
YRB	−9.91%	−2.68%	−9.44%	−3.67%	2.88%	−4.83%
HURB	−11.44%	23.23%	−10.39%	21.55%	−13.99%	27.83%
NWRB	−1.25%	11.61%	2.47%	11.47%	−6.87%	−3.24%
YZRB	7.55%	−8.64%	6.21%	−7.53%	8.72%	−12.47%
PRB	7.81%	−8.64%	8.27%	−8.41%	6.06%	−8.04%
SERB	1.94%	−12.5%	1.52%	−11.44%	−2.33%	−6.78%
SWRB	−1.94%	0.76%	−5.43%	4.55%	5.8%	−7.3%
Nation	1.79%	−5.15%	1.6%	−4.13%	3.32%	−8.25%

References

1. Elahi, E.; Khalid, Z.; Tauni, M.Z.; Zhang, H.; Lirong, X. Extreme weather events risk to crop-production and the adaptation of innovative management strategies to mitigate the risk: A retrospective survey of rural Punjab, Pakistan. *Technovation* **2022**, *117*, 102255. [CrossRef]
2. Lake, P.S.; Palmer, M.A.; Biro, P.; Cole, J.; Covich, A.P.; Dahm, C.; Gibert, J.; Goedkoop, W.; Martens, K.; Verhoeven, J.O.S. Global Change and the Biodiversity of Freshwater Ecosystems: Impacts on Linkages between Above-Sediment and Sediment Biota: All forms of anthropogenic disturbance—Changes in land use, biogeochemical processes, or biotic addition or loss—Not only damage the biota of freshwater sediments but also disrupt the linkages between above-sediment and sediment-dwelling biota. *BioScience* **2000**, *50*, 1099–1107.
3. Abbas, A.; Waseem, M.; Ullah, W.; Zhao, C.; Zhu, J. Spatiotemporal analysis of meteorological and hydrological droughts and their propagations. *Water* **2021**, *13*, 2237. [CrossRef]
4. Wijeratne, V.P.; Li, G.; Mehmood, M.S.; Abbas, A. Assessing the Impact of Long-Term ENSO, SST, and IOD Dynamics on Extreme Hydrological Events (EHEs) in the Kelani River Basin (KRB), Sri Lanka. *Atmosphere* **2022**, *14*, 79. [CrossRef]
5. Chahine, M.T. The hydrological cycle and its influence on climate. *Nature* **1992**, *359*, 373. [CrossRef]
6. Oki, T.; Kanae, S. Global hydrological cycles and world water resources. *Science* **2006**, *313*, 1068–1072. [CrossRef]
7. Nandakumar, N.; Mein, R.G. Uncertainty in rainfall—Runoff model simulations and the implications for predicting the hydrologic effects of land-use change. *J. Hydrol.* **1997**, *192*, 211–232. [CrossRef]

8. Ott, B.; Uhlenbrook, S. Quantifying the impact of land-use changes at the event and seasonal time scale using a process-oriented catchment model. *Hydrol. Earth Syst. Sci.* **2004**, *8*, 62–78. [CrossRef]
9. Devia, G.K.; Ganasri, B.P.; Dwarakish, G.S. A review on hydrological models. *Aquat. Procedia* **2015**, *4*, 1001–1007. [CrossRef]
10. Kingston, D.; Massei, N.; Dieppois, B.; Hannah, D.; Hartmann, A.; Lavers, D.; Vidal, J.P. Moving beyond the catchment scale: Value and opportunities in large-scale hydrology to understand our changing world. *Hydrol. Processes* **2020**, *34*, 2292–2298. [CrossRef]
11. Hong, Y.; Hsu, K.; Moradkhani, H.; Sorooshian, S. Uncertainty quantification of satellite precipitation estimation and Monte Carlo assessment of the error propagation into hydrologic response. *Water Resour. Res.* **2006**, *42*, W08421. [CrossRef]
12. Kim, J.; Han, H. Evaluation of the CMORPH high-resolution precipitation product for hydrological applications over South Korea. *Atmospheric Research.* **2021**, *258*, 105650. [CrossRef]
13. Rivas, R.; Caselles, V. A simplified equation to estimate spatial reference evaporation from remote sensing-based surface temperature and local meteorological data. *Remote Sens. Environ.* **2004**, *93*, 68–76. [CrossRef]
14. Lo, M.H.; Famiglietti, J.S.; Reager, J.T.; Rodell, M.; Swenson, S.; Wu, W.Y. GRACE-Based Estimates of Global Groundwater Depletion. Terrestrial Water Cycle and Climate Change: Natural and Human-Induced Impacts. In *Terrestrial Water Cycle and Climate Change: Natural and Human-Induced Impacts*; John Wiley & Sons: Hoboken, NJ, USA, 2016; pp. 135–146.
15. Gleeson, T.; Wada, Y.; Bierkens, M.F.; Van Beek, L.P. Water balance of global aquifers revealed by groundwater footprint. *Nature* **2012**, *488*, 197–200. [CrossRef] [PubMed]
16. Sheffield, J.; Ferguson, C.R.; Troy, T.J.; Wood, E.F.; McCabe, M.F. Closing the terrestrial water budget from satellite remote sensing. *Geophys. Res. Lett.* **2009**, *36*, L07403. [CrossRef]
17. Tang, G.; Behrangi, A.; Long, D.; Hong, Y. Accounting for spatiotemporal errors of gauges: A critical step to evaluate gridded precipitation products. *J. Hydrol.* **2008**, *559*, 294–306. [CrossRef]
18. Liang, X.; Lettenmaier, D.P.; Wood, E.F.; Burges, S.J. A simple hydrologically based model of land surface water and energy fluxes for general circulation models. *J. Geophys. Res. Atmos.* **1994**, *99*, 14415–14428.
19. Alcamo, J.; Döll, P.; Henrichs, T.T.; Kaspar, F.; Lehner, B.; Rösch, T.; Siebert, S. Development and testing of the WaterGAP 2 global model of water use and availability. *Hydrol. Sci. J.* **2003**, *48*, 317–337. [CrossRef]
20. Widén-Nilsson, E.; Halldin, S.; Xu, C. Global water-balance modelling with WASMOD-M: Parameter estimation and regionalisation. *J. Hydrol.* **2007**, *340*, 105–118. [CrossRef]
21. Kumar, R.; Livneh, B.; Samaniego, L. Toward computationally efficient large-scale hydrologic predictions with a multiscale regionalization scheme. *Water Resour. Res.* **2013**, *49*, 5700–5714. [CrossRef]
22. Donnelly, C.; Andersson, J.C.; Arheimer, B. Using flow signatures and catchment similarities to evaluate the E-HYPE multi-basin model across Europe. *Hydrol. Sci. J.* **2016**, *61*, 255–273. [CrossRef]
23. Schuol, J.; Abbaspour, K.C.; Yang, H.; Srinivasan, R.; Zehnder, A.J. Modeling blue and green water availability in Africa. *Water Resour. Res.* **2008**, *44*, W07406. [CrossRef]
24. Jia, Y.; Wang, H.; Zhou, Z.; Qiu, Y.; Luo, X.; Wang, J.; Yan, D.; Qin, D. Development of the WEP-L distributed hydrological model and dynamic assessment of water resources in the Yellow River basin. *J. Hydrol.* **2006**, *331*, 606–629. [CrossRef]
25. Yang, D.; Musiake, K. A continental scale hydrological model using the distributed approach and its application to Asia. *Hydrol. Processes* **2003**, *17*, 2855–2869. [CrossRef]
26. Gao, G.; Chen, D.; Xu, C.Y.; Simelton, E. Trend of estimated actual evapotranspiration over China during 1960–2002. *J. Geophys. Res. Atmos.* **2007**, *112*, D11120. [CrossRef]
27. Hao, Y.; Baik, J.; Choi, M. Combining generalized complementary relationship models with the Bayesian Model Averaging method to estimate actual evapotranspiration over China. *Agric. For. Meteorol.* **2019**, *279*, 107759. [CrossRef]
28. Zhang, Q.; Xu, C.Y.; Chen, X. Reference evapotranspiration changes in China: Natural processes or human influences? *Theor. Appl. Climatol.* **2011**, *103*, 479–488. [CrossRef]
29. Zhang, X.; Tang, Q. Combining satellite precipitation and long-term ground observations for hydrological monitoring in China. *J. Geophys. Res. Atmos.* **2015**, *120*, 6426–6443. [CrossRef]
30. Zhou, X.; Lei, W. Spatial patterns of sample entropy based on daily precipitation time series in China and their implications for land surface hydrological interactions. *Int. J. Climatol.* **2020**, *40*, 1669–1685. [CrossRef]
31. Feng, W.; Shum, C.K.; Zhong, M.; Pan, Y. Groundwater storage changes in China from satellite gravity: An overview. *Remote Sens.* **2018**, *10*, 674. [CrossRef]
32. Bai, P.; Liu, X.; Liu, C. Improving hydrological simulations by incorporating GRACE data for model calibration. *J. Hydrol.* **2018**, *557*, 291–304. [CrossRef]
33. Li, D.; Wang, W.; Hu, S.; Li, Y. Characteristics of annual runoff variation in major rivers of China. *Hydrol. Processes* **2012**, *26*, 2866–2877. [CrossRef]
34. Wang, G.; Zhang, J.; He, R.; Liu, C.; Ma, T.; Bao, Z.; Liu, Y. Runoff sensitivity to climate change for hydro-climatically different catchments in China. *Stoch. Environ. Res. Risk Assess.* **2017**, *31*, 1011–1021. [CrossRef]
35. Guan, X.; Zhang, J.; Bao, Z.; Liu, C.; Jin, J.; Wang, G. Past variations and future projection of runoff in typical basins in 10 water zones, China. *Sci. Total Environ.* **2021**, *798*, 149277. [CrossRef]
36. Miao, Y.; Wang, A. A daily $0.25° \times 0.25°$ hydrologically based land surface flux dataset for conterminous China, 1961–2017. *J. Hydrol.* **2020**, *590*, 125413. [CrossRef]

37. Sun, S.; Bi, Z.; Zhou, S.; Wang, H.; Li, Q.; Liu, Y.; Wang, G.; Li, S.; Chen, H.; Zhou, Y. Spatiotemporal shifts in key hydrological variables and dominant factors over China. *Hydrol. Processes* **2021**, *35*, E14319. [CrossRef]
38. Liu, H.; Jia, Y.; Niu, C.; Hu, P.; Du, J.; Su, H.; Zeng, Q. Evolution of Main Water Cycle Fluxes in the Karst Mountain Region of Southwest China. *Water* **2020**, *12*, 2262.
39. Liu, B.; Speed, R. Water Resources Management in the People's Republic of China. *Int. J. Water Resour. Dev.* **2009**, *25*, 193–208. [CrossRef]
40. Xia, J.; Chen, J.; Weng, J.; Yu, L.; Qi, J.; Liao, Q. Vulnerability of water resources and its spatial heterogeneity in Haihe River Basin, China. *Chin. Geogr. Sci.* **2014**, *24*, 525–539. [CrossRef]
41. Yan, J.; Jia, S.; Lv, A.; Zhu, W. Water resources assessment of China's transboundary river basins using a machine learning approach. *Water Resour. Res.* **2019**, *55*, 632–655. [CrossRef]
42. China Meteorological Administration Meteorological Data Centre. 2019. Available online: https://data.cma.cn/ (accessed on 4 May 2019).
43. Ministry of Water Resources of the People's Republic of China. *Annual Hydrological Report of the People's Republic of China*; Shandong Hydrology Press: Weifang, China, 2015.
44. Liu, H.; Jia, Y.; Niu, C.; Su, H.; Wang, J.; Du, J.; Khaki, M.; Hu, P.; Liu, J. Development and validation of a physically-based, national-scale hydrological model in China. *J. Hydrol.* **2020**, *590*, 125431. [CrossRef]
45. Liu, H.; Du, J.; Jia, Y.; Liu, J.; Niu, C.; Gan, Y. Improvement of watershed subdivision method for large scale regional distributed hydrology mode. *Adv. Eng. Sci.* **2019**, *51*, 36–44.
46. Monteith, J.L. Evaporation and environment. In *The State and Movement of Water in Living Organisms*; Fogg, G.E., Ed.; Cambridge University Press: Cambridge, UK, 1965; pp. 205–234.
47. Penman, H.L. Natural evaporation from open water, bare soil and grass. *Proc. R. Soc. London Ser. A Math. Phys. Sci.* **1948**, *193*, 120–145.
48. Chen, L.; Young, M.H. Green-Ampt infiltration model for sloping surfaces. *Water Resour. Res.* **2006**, *42*, W07420. [CrossRef]
49. Kendall, M.G. *Rank Correlation Measures*; Charles Griffin Book Series; Oxford University Press: London, UK, 1975; Volume 202, p. 15.
50. Hamed, K.H. Trend detection in hydrologic data: The Mann–Kendall trend test under the scaling hypothesis. *J. Hydrol.* **2008**, *349*, 350–363. [CrossRef]
51. Gocic, M.; Trajkovic, S. Analysis of changes in meteorological variables using Mann-Kendall and Sen's slope estimator statistical tests in Serbia. *Glob. Planet. Chang.* **2013**, *100*, 172–182. [CrossRef]
52. Liu, H. Development and Application of Distributed Hydrological Model at the China National Scale Considering the Spatial Difference of Runoff Generation Mechanisms. Ph.D. Thesis, China Institute of Water Resources & Hydropower Research (IWHR), Beijing, China, 2019. (In Chinese).
53. Abbott, B.W.; Bishop, K.; Zarnetske, J.P.; Minaudo, C.; Chapin III, F.S.; Krause, S.; Hannah, D.M.; Conner, L.; Ellison, D.; Godsey, S.E.; et al. Human domination of the global water cycle absent from depictions and perceptions. *Nat. Geosci.* **2019**, *12*, 533–540. [CrossRef]
54. Li, X.; Li, Y.; Chen, A.; Gao, M.; Slette, I.J.; Piao, S. The impact of the 2009/2010 drought on vegetation growth and terrestrial carbon balance in Southwest China. *Agric. For. Meteorol.* **2019**, *269*, 239–248. [CrossRef]
55. Gao, H.; Wang, J.; Yang, Y.; Pan, X.; Ding, Y.; Duan, Z. Permafrost hydrology of the Qinghai-Tibet Plateau: A review of processes and modeling. *Front. Earth Sci.* **2021**, *8*, 576838. [CrossRef]
56. Lei, Y.; Yao, T.; Yang, K.; Sheng, Y.; Kleinherenbrink, M.; Yi, S.; Bird, B.W.; Zhang, X.; Zhu, L.; Zhang, G. Lake seasonality across the Tibetan Plateau and their varying relationship with regional mass changes and local hydrology. *Geophys. Res. Lett.* **2017**, *44*, 892–900. [CrossRef]
57. Luo, Y.; Wang, X.; Piao, S.; Sun, L.; Ciais, P.; Zhang, Y.; Ma, C.; Gan, R.; He, C. Contrasting streamflow regimes induced by melting glaciers across the Tien Shan–Pamir–North Karakoram. *Sci. Rep.* **2018**, *8*, 16470. [CrossRef] [PubMed]
58. Du, J.Q.; Quan, Z.J.; Fang, S.F.; Liu, C.; Wu, J.; Fu, Q. Spatiotemporal changes in vegetation coverage and its causes in China since the Chinese economic reform. *Environ. Sci. Pollut. Res.* **2020**, *27*, 1144–1159. [CrossRef] [PubMed]
59. Wang, L.; Wang, S.; Zhou, Y.; Liu, W.; Hou, Y.; Zhu, J.; Wang, F. Mapping population density in China between 1990 and 2010 using remote sensing. *Remote Sens. Environ.* **2018**, *210*, 269–281. [CrossRef]
60. Zhang, B.; Cui, H.S.; Yu, L.; He, Y.F. Land reclamation process in northeast China since 1900. *Chin. Geogr. Sci.* **2003**, *13*, 119–123. [CrossRef]
61. Feng, X.; Fu, B.; Piao, S.; Wang, S.; Ciais, P.; Zeng, Z.; Lü, Y.; Zeng, Y.; Li, Y.; Jiang, X.; et al. Revegetation in China's Loess Plateau is approaching sustainable water resource limits. *Nat. Clim. Chang.* **2016**, *6*, 1019–1022. [CrossRef]
62. Yue, X.; Mu, X.; Zhao, G.; Shao, H.; Gao, P. Dynamic changes of sediment load in the middle reaches of the Yellow River basin, China and implications for eco-restoration. *Ecol. Eng.* **2014**, *73*, 64–72. [CrossRef]
63. Kirkham, M.B. Leaf Anatomy and Leaf Elasticity. In *Principles of Soil and Plant Water Relations*, 2nd ed.; Academic Press: Boston, MA, USA, 2014; pp. 409–430.
64. McVicar, T.R.; Roderick, M.L.; Donohue, R.J.; Li, L.T.; Van Niel, T.G.; Thomas, A.; Grieser, J.; Jhajharia, D.; Himri, Y.; Mahowald, N.M.; et al. Global review and synthesis of trends in observed terrestrial near-surface wind speeds: Implications for evaporation. *J. Hydrol.* **2012**, *416*, 182–205. [CrossRef]
65. Budyko, M.I. *Climate and Life*; Academic: San Diego, CA, USA, 1974.

66. Wang, H.; Li, Z.; Cao, L.; Feng, R.; Pan, Y. Response of NDVI of natural vegetation to climate changes and drought in China. *Land* **2021**, *10*, 966. [CrossRef]
67. Tang, X.L.; Lv, X.; He, Y. Features of climate change and their effects on glacier snow melting in Xinjiang, China. *Comptes Rendus Geosci.* **2013**, *345*, 93–100. [CrossRef]
68. Zhang, M.; Ren, Q.; Wei, X.; Wang, J.; Yang, X.; Jiang, Z. Climate change, glacier melting and streamflow in the Niyang River Basin, Southeast Tibet, China. *Ecohydrology* **2011**, *4*, 288–298. [CrossRef]
69. FAO (Food and Agriculture Organization). *Review of the World Water Resources by Country*; Water Report No. 23; FAO: Rome, Italy, 2003.
70. Ministry of Water Resources of the People's Republic of China. *China Water Resources Bulletin*; Ministry of Water Resources of the People's Republic of China: Beijing, China, 2019.
71. Wang, J.; Li, Y.; Huang, J.; Yan, T.; Sun, T. Growing water scarcity, food security and government responses in China. *Glob. Food Secur.* **2017**, *14*, 9–17. [CrossRef]
72. Xu, Z.; Chen, X.; Wu, S.R.; Gong, M.; Du, Y.; Wang, J.; Li, Y.; Liu, J. Spatial-temporal assessment of water footprint, water scarcity and crop water productivity in a major crop production region. *J. Clean. Prod.* **2019**, *224*, 375–383. [CrossRef]
73. Zhao, Z.Y.; Zuo, J.; Zillante, G. Transformation of water resource management: A case study of the South-to-North Water Diversion project. *J. Clean. Prod.* **2017**, *163*, 136–145. [CrossRef]
74. Zhao, J.; Ni, H.; Peng, X.; Li, J.; Chen, G.; Liu, J. Impact of water price reform on water conservation and economic growth in China. *Econ. Anal. Policy* **2016**, *51*, 90–103. [CrossRef]
75. Chen, Y.; Zhu, M.; Lu, J.; Zhou, Q.; Ma, W. Evaluation of ecological city and analysis of obstacle factors under the background of high-quality development: Taking cities in the Yellow River Basin as examples. *Ecol. Indic.* **2020**, *118*, 106771. [CrossRef]
76. Jiang, L.; Zuo, Q.; Ma, J.; Zhang, Z. Evaluation and prediction of the level of high-quality development: A case study of the Yellow River Basin, China. *Ecol. Indic.* **2021**, *129*, 107994. [CrossRef]
77. Gao, C.; Zhang, Z.; Zhai, J.; Qing, L.; Mengting, Y. Research on meteorological thresholds of drought and flood disaster: A case study in the Huai River Basin, China. *Stoch. Environ. Res. Risk Assess.* **2015**, *29*, 157–167. [CrossRef]
78. Song, K.; Wang, Z.; Li, L.; Tedesco, L.; Li, F.; Jin, C.; Du, J. Wetlands shrinkage, fragmentation and their links to agriculture in the Muleng–Xingkai Plain, China. *J. Environ. Manag.* **2012**, *111*, 120–132. [CrossRef]
79. Xiang, H.; Wang, Z.; Mao, D.; Zhang, J.; Xi, Y.; Du, B.; Zhang, B. What did China's National Wetland Conservation Program Achieve? Observations of changes in land cover and ecosystem services in the Sanjiang Plain. *J. Environ. Manag.* **2020**, *267*, 110623. [CrossRef]
80. Liang, J.; Yang, Z.; Lin, P. Systematic Hydrological Evaluation of the Noah-MP Land Surface Model over China. *Adv. Atmos. Sci.* **2019**, *36*, 1171–1187. [CrossRef]
81. Li, Y.; Piao, S.; Li, L.Z.X.; Chen, A.; Wang, X.; Ciais, P.; Huang, L.; Lian, X.; Peng, S.; Zeng, Z.; et al. Divergent hydrological response to large-scale afforestation and vegetation greening in China. *Sci. Adv.* **2018**, *4*, eaar4182. [CrossRef] [PubMed]